SIMULATING DAMAGE AND PERMANENT STRAIN IN FIBRE-REINFORCED COMPOSITES UNDER IN-PLANE FATIGUE LOADING

W. Van Paepegem[1] and J. Degrieck[1]

[1] Department of Mechanical Construction and Production, Ghent University
Sint-Pietersnieuwstraat 41, Gent, Belgium

ABSTRACT

Fibre-reinforced composites are used in many fatigue-critical applications (wind turbine blades, aircraft components, leaf springs,...). Due to their heterogeneous and anisotropic nature, their fatigue behaviour is rather complex and several damage mechanisms can develop during fatigue life. This paper presents a damage mechanics based fatigue model for fibre-reinforced plastics, where both stiffness degradation and (possible) accumulation of permanent strain are simulated from the first loading cycle up till final failure. The model has been validated for cantilever bending fatigue tests of plain woven glass/epoxy composite with two different stacking sequences. Although the damage growth rate varies along the specimen length, the finite element simulations with the damage model are able to account for decreasing (bending) stiffness and permanent strain.

1. INTRODUCTION

The existing fatigue models for fibre-reinforced composites can generally be classified into [1]: (i) fatigue life models (S-N curves), (ii) damage accumulation models ('mechanistic models'), and (iii) phenomenological residual stiffness/strength models. The scope of most models is limited to one-dimensional fatigue loading, although some models have been applied to multi-axial fatigue loading.

In the category of fatigue life models, the multi-axial loading problem is often handled by introducing a static failure criterion (e.g. Tsai-Wu, Tsai-Hill) and replacing the static strengths with the fatigue strengths in the criterion. This approach was followed by Lawrence Wu [2], Jen and Lee [3,4] and Philippidis and Vassilopoulos [5]. The drawback of this approach is that the fatigue strengths must be determined experimentally for different stress amplitudes, stress ratios and bi-axiality ratios. This requires a large experimental input of S-N curves which represent directly the perceived nature of fatigue in terms of experimental results, but give no indication of the mechanisms of fatigue damage, of the presence or behaviour of cracks, or of changes in the characteristics of the material as a consequence of the fatigue process. Well-known mechanistic models for multi-axial fatigue loading are the continuum damage models by Talreja [6,7], Allen et al. [8,9] and Sedrakian et al. [10,11]. Recently, Shokrieh and Lessard [12,13] proposed a so-called 'generalized residual material property degradation model' for unidirectionally reinforced laminates which uses Hashin-type fatigue failure criteria to determine the damage mode and consequently reduces the corresponding elastic properties.

In this paper, the phenomenological residual stiffness approach is adopted to simulate stiffness degradation, stress redistribution and permanent strain in fibre-reinforced polymers under generalized in-plane loading. The presence of each of these phenomena was clearly indicated by the experimental results which were obtained from displacement-controlled bending fatigue tests on plain woven glass/epoxy composites.

2. EXPERIMENTAL SETUP

Fig. 1 shows the experimental setup for displacement-controlled cantilever bending fatigue tests. The shaft (point D in Fig. 1) bears a mechanism with crank and connecting rod, which imposes an alternating displacement on the hinge (point C in Fig. 1) that connects the connecting rod with the moving clamp of the composite specimen.

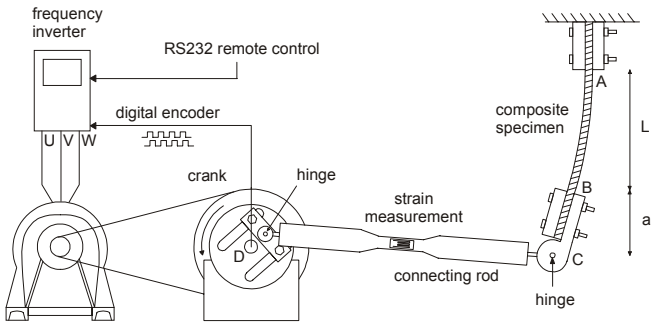

Fig. 1. Schematic drawing of the experimental setup.

At the upper end the specimen is clamped (point A in Fig. 1). Hence the sample is loaded as a composite cantilever beam. The force necessary to bend the specimen, is measured by means of a strain-gauge bridge on the connecting rod. The testing frequency is 2.2 Hz.
The amplitude u_{max} of the prescribed displacement is defined as the orthogonal distance between the centre of the hinge (point C in Fig. 1) and the vertical line passing through the midplane of the undeformed specimen. The amplitude u_{max} can be adjusted by changing the position of the crank.
The selected material was a plain woven glass fabric/epoxy composite, because of its widespread application in industry [14,15]. For the first stacking sequence, the warp direction of all eight layers was aligned with the loading direction (denoted as $[\#0^o]_8$, where '0°' means that the warp direction of each of the eight layers has been aligned with the loading direction and where the hash mark '#' refers to the fabric reinforcement type). For the second stacking sequence, the angle between the warp direction of all layers and the loading direction was 45º (denoted as $[\#45^o]_8$). The two stacking sequences are supposed to represent two fundamentally different stress states. The bending of the $[\#0°]_8$ stacking sequence results in a quasi one-dimensional loading of the laminate, with large stresses along the longitudinal fibre direction. In the $[\#45°]_8$ stacking sequence, the load is sustained by a combined state of normal stresses in the two fibre directions of the fabric, and shear stresses.
The material was fabricated by resin transfer moulding, and a full characterization of the composite material was performed. All specimens had a fibre volume fraction of 0.48 and a thickness of 2.72 mm. They were cut to dimensions of 145 mm long by 30 mm wide.

3. EXPERIMENTAL OBSERVATIONS

Fig. 2 shows the force-cycle history for a $[\#0°]_8$ and $[\#45^o]_8$ specimen, subjected to single-sided bending with u_{max} = 34.4 mm. The abscissa contains the number of cycles; the ordinate axis shows the force [Newton], which is measured by the strain gauge bridge on the connecting rod (Fig. 1) during the fatigue tests.

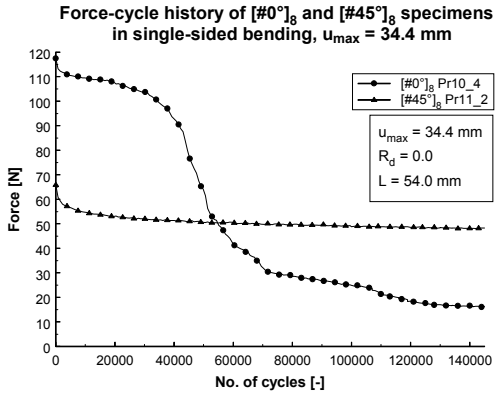

Fig. 2. Force-cycle histories for $[\#0°]_8$ and $[\#45°]_8$ specimens (single-sided bending, u_{max} = 34.4 mm).

The $[\#0°]_8$ specimens degrade gradually in the early loading cycles, but their stiffness is reduced significantly after about 40,000 cycles. The initial force on the $[\#45°]_8$ specimen is smaller, because its stiffness is lower. However, after 50,000 cycles, its remaining stiffness has become larger than that of the $[\#0°]_8$ specimen. Of course the ratio of the surface strain to the ultimate strain is different for the two specimens. The Tsai-Wu failure criterion will reach its failure value much earlier for the $[\#0°]_8$ specimen than for the $[\#45°]_8$ specimen, because the stresses, resulting from the imposed curvature, are smaller for the $[\#45°]_8$ specimen.
Another aspect which should be paid attention to, is the accumulation of permanent strain for the $[\#45°]_8$ specimens under large prescribed displacements. Indeed, when u_{max} is large, a substantial permanent deformation did remain after removing the grips from the $[\#45°]_8$ specimens, while this was much less the case for the $[\#0°]_8$ specimens.
Fig. 3 shows the out-of-plane displacement profiles for the $[\#45°]_8$ specimen Pr11_3 during fatigue life and after removing the lower clamp for u_{max} = 37.8 mm. These out-of-plane displacement profiles have been recorded with the developed digital phase-shift shadow moiré technique [16]. As can be seen from the Figure, the permanent deformation is not at all negligible. The right photograph shows a picture of the $[\#45°]_8$ specimens Pr06_3, Pr06_4 and Pr06_5, after having been subjected to a prescribed displacement u_{max} of 38.9 mm for about 900,000 loading cycles. The specimen at the right-hand side of the picture is an undamaged specimen for comparison purpose.

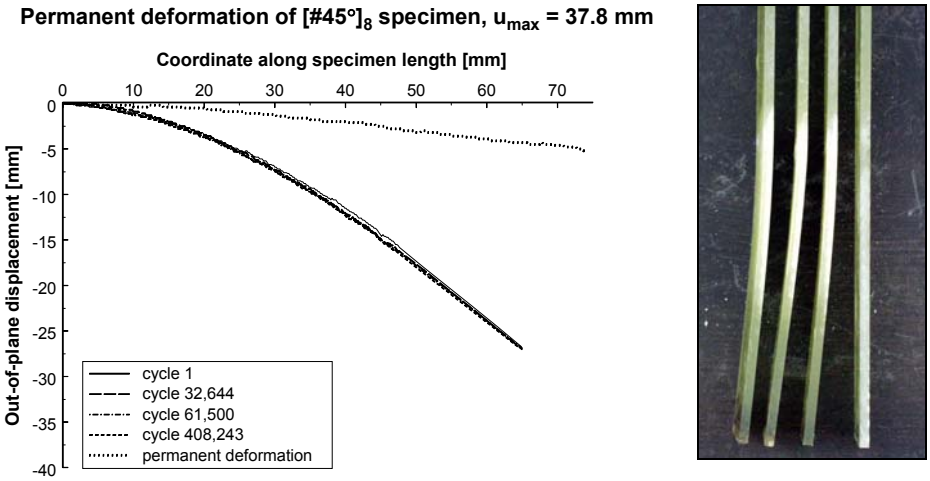

Fig. 3. Out-of-plane displacement profiles of $[\#45°]_8$ specimen Pr11_3 during fatigue life (u_{max} = 37.8 mm) (left) and permanent deformation of $[\#45°]_8$ specimens after removing the lower clamp (right).

4. FATIGUE DAMAGE MODEL

4.1 General Description

In order to simulate these experimentally observed phenomena, the model should be able to simulate: (i) stiffness degradation (decreasing bending force), (ii) stress redistribution (changing bending profiles), and (iii) accumulation of permanent strain.
To that purpose, a residual stiffness model was developed with three damage variables: D_{11} (damage in the $\vec{e}_{11}$ direction), D_{22} (damage in the $\vec{e}_{22}$ direction), and D_{12} (shear damage). These damage variables are directly related with the corresponding stress components σ_{11} (positive/negative), σ_{22} (positive/negative) and σ_{12} in the orthotropic directions of the glass/epoxy composite. For each of the three damage variables, the growth rate per fatigue cycle N is defined by a differential equation $d(D_{ij})/dN$. To make a prediction of the moment of failure, the governing stresses σ_{11}, σ_{22} and σ_{12} in the corresponding differential equations have been replaced by the newly defined *fatigue failure indices* Σ_{11}, Σ_{22} en Σ_{12}. These failure indices are calculated from the Tsai-Wu static failure criterion, where the nominal stresses

σ_{11}, σ_{22}, and σ_{12} are replaced by the effective stresses $\widetilde{\sigma}_{11}$, $\widetilde{\sigma}_{22}$ and $\widetilde{\sigma}_{12}$. As such, there is a correlation with residual strength, and the moment of failure in the displacement-controlled bending fatigue tests can be predicted as well.
Finally, the permanent strains ε_{ii}^{p} (i=1,2) have been introduced. The growth rate $d(\varepsilon_{ii}^{p})/dN$ is proportional with the elastic strain ε_{ii} and the growth rate $d(D_{12})/dN$.

4.2 Relevant Equations

Three relationships make up the complete modelling framework: (i) the damage-stiffness relationships, (ii) the fatigue damage evolution laws $d(D_{ij})/dN$, and (iii) the growth laws for the permanent strains ε_{ii}^{p}. These three relationships are discussed in the following paragraphs. A detailed justification of all equations is beyond the scope of this paper and has been the result of a larger research programme which can be found in Reference [17].

4.2.1 Damage-stiffness Relationships

It is first postulated that there is a distinct difference between the damage kinetics of intra-layer damage (matrix cracks, fibre/matrix debonding, fibre fracture,…) and inter-layer damage (delaminations). Moreover the responsible stress components are not the same. The in-plane stresses (σ_{11}, σ_{22} and σ_{12}) are affecting the intra-layer damage, while the out-of-plane stresses (σ_{13}, σ_{23} and σ_{33}) are causing inter-layer damage. It is clear that the one-dimensional fatigue damage model developed so far, is modelling the intra-layer damage types. Delaminations were not taken into account and the stacking sequence was chosen such that delaminations did not develop under the experimental loading conditions.
If only intra-layer damage is considered, it is postulated that there exist three damage variables D_{11}, D_{22} and D_{12}, which are defined through the relations:

$$\begin{Bmatrix}\sigma_{11}\\ \sigma_{22}\\ \sigma_{33}\\ \sigma_{23}\\ \sigma_{13}\\ \sigma_{12}\end{Bmatrix} = \begin{bmatrix}\sqrt{1-D_{11}} & 0 & 0 & 0 & 0 & 0\\ 0 & \sqrt{1-D_{22}} & 0 & 0 & 0 & 0\\ 0 & 0 & 1 & 0 & 0 & 0\\ 0 & 0 & 0 & 1 & 0 & 0\\ 0 & 0 & 0 & 0 & 1 & 0\\ 0 & 0 & 0 & 0 & 0 & \sqrt{1-D_{12}}\end{bmatrix} \cdot \begin{bmatrix}C_{11} & C_{12} & C_{13} & 0 & 0 & 0\\ C_{12} & C_{22} & C_{23} & 0 & 0 & 0\\ C_{13} & C_{23} & C_{33} & 0 & 0 & 0\\ 0 & 0 & 0 & C_{44} & 0 & 0\\ 0 & 0 & 0 & 0 & C_{55} & 0\\ 0 & 0 & 0 & 0 & 0 & C_{66}\end{bmatrix} \cdot \begin{bmatrix}\sqrt{1-D_{11}} & 0 & 0 & 0 & 0 & 0\\ 0 & \sqrt{1-D_{22}} & 0 & 0 & 0 & 0\\ 0 & 0 & 1 & 0 & 0 & 0\\ 0 & 0 & 0 & 1 & 0 & 0\\ 0 & 0 & 0 & 0 & 1 & 0\\ 0 & 0 & 0 & 0 & 0 & \sqrt{1-D_{12}}\end{bmatrix} \cdot \begin{Bmatrix}\varepsilon_{11}-\varepsilon_{11}^{p}\\ \varepsilon_{22}-\varepsilon_{22}^{p}\\ \varepsilon_{33}\\ 2\varepsilon_{23}\\ 2\varepsilon_{13}\\ 2\varepsilon_{12}\end{Bmatrix} \tag{1}$$

where [C] is the initial orthotropic stiffness matrix of the composite material. The permanent strains ε_{11}^{p} and ε_{22}^{p} must account for the permanent deformation of the $[\#45°]_8$ specimens (see Fig. 3). Although this Equation represents a simplified approach, it is at least manageable in terms of number of damage variables and finite element implementation, because the symmetry of the stiffness matrix [C] is guaranteed at any time during fatigue life.
A very important advantage of the formulation in Eq. (1) is that the damage variables D_{11}, D_{22} and D_{12} are directly related with their respective stress components σ_{11}, σ_{22} and σ_{12}. As such, the damage growth rates dD_{11}/dN, dD_{22}/dN and dD_{12}/dN are driven by the respective stresses σ_{11}, σ_{22} and σ_{12}. Further, there is a very clear distinction between positive and negative stresses for each of the damage variables. Indeed, for each damage variable, the sign of the

corresponding stress component dictates which damage growth rate equation should be used, the one for tension or the one for compression.

4.2.2 Fatigue Damage Evolution Laws

The final objective is the development of a set of damage growth rate equations of the form:

$$\frac{dD_{11}}{dN} = \begin{cases} f_1(\sigma_{ij}, D_{ij}) & \text{if } \sigma_{11} \geq 0 \\ f_2(\sigma_{ij}, D_{ij}) & \text{if } \sigma_{11} < 0 \end{cases}$$

$$\frac{dD_{22}}{dN} = \begin{cases} g_1(\sigma_{ij}, D_{ij}) & \text{if } \sigma_{22} \geq 0 \\ g_2(\sigma_{ij}, D_{ij}) & \text{if } \sigma_{22} < 0 \end{cases} \tag{2}$$

$$\frac{dD_{12}}{dN} = h(\sigma_{ij}, D_{ij})$$

Each damage growth rate equation should depend on the multi-axial in-plane stress state σ_{ij} and the actual value of the damage variables D_{ij}. As the stress components σ_{ij} give no indication of reserve to failure, new stress measures have been developed [18]. The *fatigue failure indices* Σ_{ij}^{2D} $(i, j = 1,2)$ for generalized in-plane fatigue loading can be calculated from the Tsai-Wu static failure criterion by replacing the nominal stresses σ_{ij} with the stresses $\sigma_{ij}/(1\text{-}D_{ij})$. The corresponding fatigue failure index Σ_{11}^{2D} for the stress component σ_{11} is defined as the positive root of the Eq. [18]:

$$\left(\frac{1}{X_T} - \frac{1}{|X_C|}\right)\frac{\sigma_{11}}{\Sigma_{11}^{2D}\cdot(1-D_{11})} + \left(\frac{1}{Y_T} - \frac{1}{|Y_C|}\right)\frac{\sigma_{22}}{1-D_{22}} + \frac{1}{X_T\cdot|X_C|}\left(\frac{\sigma_{11}}{\Sigma_{11}^{2D}\cdot(1-D_{11})}\right)^2 + \frac{1}{Y_T\cdot|Y_C|}\left(\frac{\sigma_{22}}{1-D_{22}}\right)^2 + \frac{1}{S^2}\left(\frac{\sigma_{12}}{1-D_{12}}\right)^2 = 1 \tag{3}$$

The fatigue failure index Σ_{22}^{2D} for the stress component σ_{22} is defined as the positive root of the Eq. [18]:

$$\left(\frac{1}{X_T} - \frac{1}{|X_C|}\right)\frac{\sigma_{11}}{1-D_{11}} + \left(\frac{1}{Y_T} - \frac{1}{|Y_C|}\right)\frac{\sigma_{22}}{\Sigma_{22}^{2D}\cdot(1-D_{22})} + \frac{1}{X_T\cdot|X_C|}\left(\frac{\sigma_{11}}{1-D_{11}}\right)^2 + \frac{1}{Y_T\cdot|Y_C|}\left(\frac{\sigma_{22}}{\Sigma_{22}^{2D}\cdot(1-D_{22})}\right)^2 + \frac{1}{S^2}\left(\frac{\sigma_{12}}{1-D_{12}}\right)^2 = 1 \tag{4}$$

Finally, the fatigue failure index Σ_{12}^{2D} for the stress component σ_{12} is defined as the positive root of the Eq. [18]:

$$\left(\frac{1}{X_T}-\frac{1}{|X_C|}\right)\frac{\sigma_{11}}{1-D_{11}}+\left(\frac{1}{Y_T}-\frac{1}{|Y_C|}\right)\frac{\sigma_{22}}{1-D_{22}}+\frac{1}{X_T\cdot|X_C|}\left(\frac{\sigma_{11}}{1-D_{11}}\right)^2 + \frac{1}{Y_T\cdot|Y_C|}\left(\frac{\sigma_{22}}{1-D_{22}}\right)^2+\frac{1}{S^2}\left(\frac{\sigma_{12}}{\Sigma_{12}^{2D}\cdot(1-D_{12})}\right)^2=1 \tag{5}$$

These *fatigue failure indices* Σ_{11}^{2D}, Σ_{22}^{2D} and Σ_{12}^{2D} quantify the directional reserves to failure in in-plane loading conditions, taking into account the present damage state (D_{11}, D_{22}, D_{12}).
To assess the *relative importance of the separate stress components* σ_{ij} in the failure event, it is better to correlate the failure indices $\Sigma_{ij}^{2D}\,(i,j=1,2)$ with their one-dimensional equivalent. Also, the failure indices must reduce to their one-dimensional equivalent if the other stress components are zero.
A definition which satisfies these requirements, is the following:

$$\begin{aligned}\Sigma_{11} &= \frac{\Sigma_{11}^{2D}}{1+(\Sigma_{11}^{2D}-\Sigma_{11}^{1D})}\\ \Sigma_{22} &= \frac{\Sigma_{22}^{2D}}{1+(\Sigma_{22}^{2D}-\Sigma_{22}^{1D})}\\ \Sigma_{12} &= \frac{\Sigma_{12}^{2D}}{1+(\Sigma_{12}^{2D}-\Sigma_{12}^{1D})}\end{aligned} \tag{6}$$

The failure indices Σ_{11}^{2D}, Σ_{22}^{2D} and Σ_{12}^{2D} are calculated from the respective Eqs. (3), (4) and (5), while the one-dimensional failure indices Σ_{11}^{1D}, Σ_{22}^{1D} and Σ_{12}^{1D} are defined as the ratio of the effective stress $\tilde{\sigma}$ to the respective static strength. So, the two-dimensional failure indices $\Sigma_{ij}^{2D}\,(i,j=1,2)$ take into account the adverse effect of multi-axial loading, while the correlation with the one-dimensional ratio $\Sigma_{ij}^{1D}\,(i,j=1,2)$ to their respective static strengths indicates the relative probability of failure along the considered direction $\vec{e}_{11}$ or $\vec{e}_{22}$. The newly defined failure indices reduce to their one-dimensional equivalent if a one-dimensional stress is applied, so the relation between one-dimensional and multi-dimensional failure indices remains consistent in use.
It is important to observe that if the stress state approaches the Tsai-Wu failure surface, not all failure indices Σ_{ij} (i, j = 1,2) will reach the failure value 1.0, because the failure indices are normalized with respect to their one-dimensional ratio $\Sigma_{ij}^{1D}\,(i,j=1,2)$. To avoid any singularities in the Eqs. (3), (4) and (5) during fatigue life simulation, the calculation strategy is as follows:

- if one of the failure indices Σ_{ij} (i, j = 1,2) has a high value, the corresponding damage variable D_{ij} will grow very rapidly,
- if this failure index Σ_{ij} approaches its failure value 1.0, the corresponding stress σ_{ij} is set to zero,
- in the next evaluation of the Tsai-Wu failure indices, all terms in the stress component σ_{ij} are zero.

A detailed discussion of the damage-dependent directional failure indices Σ_{ij} can be found in [18].

In the end the close feedback between experimental observations and finite element predictions has lead to the final damage growth rate equations for generalized in-plane fatigue loading [17]:

$$\frac{dD_{11}}{dN} = \begin{cases} c_1 \cdot (1 + D_{12}^2) \cdot \Sigma_{11} \cdot \exp\left(- c_2 \dfrac{D_{11}}{\sqrt{\Sigma_{11}} \cdot (1 + D_{12}^2)} \right) & \text{if } \sigma_{11} \geq 0 \\ + c_3 \cdot D_{11} \cdot \Sigma_{11}^2 \cdot \left[1 + \exp\left(c_5 \left(\Sigma_{11} - c_4 \right) \right) \right] & \\ \left[c_1 \cdot (1 + D_{12}^2) \cdot \Sigma_{11} \cdot \exp\left(- c_2 \dfrac{D_{11}}{\sqrt{\Sigma_{11}} \cdot (1 + D_{12}^2)} \right) \right]^{1 + 2 \cdot \exp(-D_{12})} & \text{if } \sigma_{11} < 0 \\ + c_3 \cdot D_{11} \cdot \Sigma_{11}^2 \cdot \left[1 + \exp\left(\dfrac{c_5}{3} \left(\Sigma_{11} - c_4 \right) \right) \right] & \end{cases}$$

$$\frac{dD_{22}}{dN} = \begin{cases} c_1 \cdot (1 + D_{12}^2) \cdot \Sigma_{22} \cdot \exp\left(- c_2 \dfrac{D_{22}}{\sqrt{\Sigma_{22}} \cdot (1 + D_{12}^2)} \right) & \text{if } \sigma_{22} \geq 0 \\ + c_3 \cdot D_{22} \cdot \Sigma_{22}^2 \cdot \left[1 + \exp\left(c_5 \left(\Sigma_{22} - c_4 \right) \right) \right] & \\ \left[c_1 \cdot (1 + D_{12}^2) \cdot \Sigma_{22} \cdot \exp\left(- c_2 \dfrac{D_{22}}{\sqrt{\Sigma_{22}} \cdot (1 + D_{12}^2)} \right) \right]^{1 + 2 \cdot \exp(-D_{12})} & \text{if } \sigma_{22} < 0 \\ + c_3 \cdot D_{22} \cdot \Sigma_{22}^2 \cdot \left[1 + \exp\left(\dfrac{c_5}{3} \left(\Sigma_{22} - c_4 \right) \right) \right] & \end{cases}$$

$$\frac{dD_{12}}{dN} = c_1 \cdot \Sigma_{12} \cdot \exp\left(- c_2 \frac{D_{12}}{2\sqrt{\Sigma_{12}}} \right) \tag{7}$$

4.2.3 Growth Laws for Permanent Strains

Finally, additional equations for the growth rate of the permanent strains ε_{ii}^p (i = 1,2) must be established. The corresponding growth laws for the permanent strain have been written as (no summation convention) [17]:

$$\frac{d\varepsilon_{ii}^p}{dN} = \begin{cases} c_6 \cdot \varepsilon_{ii} \cdot \dfrac{dD_{12}}{dN} & \text{if } \sigma_{ii} \geq 0 \\ 0 & \text{if } \sigma_{ii} < 0 \end{cases} \qquad (i = 1,2) \tag{8}$$

The factor c_6 has been determined such that the predicted out-of-plane displacement profile after unloading matches the experimentally recorded one for the $[\#45°]_8$ specimen Pr06_1. This was the case for $c_6 = 0.6$. This implies that, if the damage D_{12} reaches its failure value 1.0, the permanent strain ε_{ii}^p cannot be larger than 60 % of the total strain amplitude ε_{ii}.

5. EXAMPLE OF FINITE ELEMENT SIMULATION

The finite element simulation concerns the bending fatigue test Pr06_3, which was performed for u_{max} = 38.9 mm. As can be seen from Fig. 4, the initial force degradation is really large, about 25 Newton.

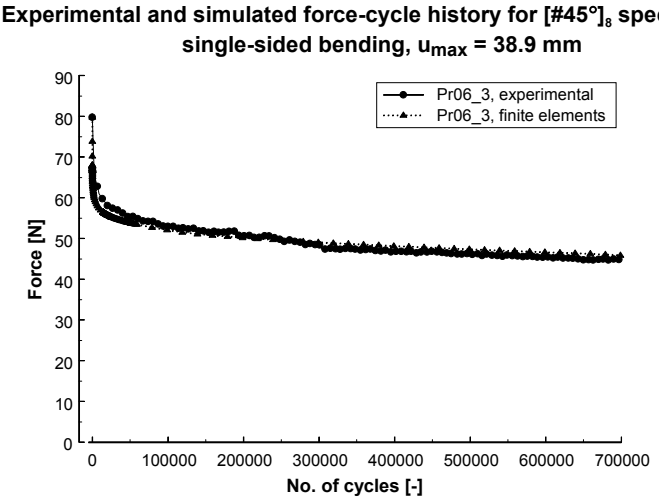

Fig. 4. Experimental and simulated force-cycle history for the $[\#45°]_8$ specimen Pr06_3 (u_{max} = 38.9 mm).

Also, the permanent deformation has increased even more, due to the larger prescribed displacement. Fig. 5 shows the experimental and simulated permanent deformation for the Pr06_3 specimen.

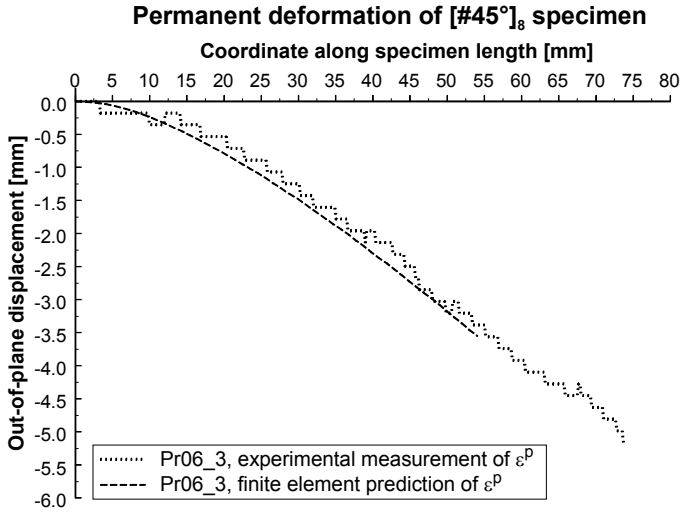

Fig. 5. Experimental and predicted permanent deformation of $[\#45°]_8$ specimen Pr06_3.

Fig. 6 shows the simulated distribution of the stress σ_{11} at the clamped cross-section at several stages during fatigue life. The accumulation of permanent strain at the tensile side causes the initial stresses to decrease much more than the stresses at the compressive side of the specimen.

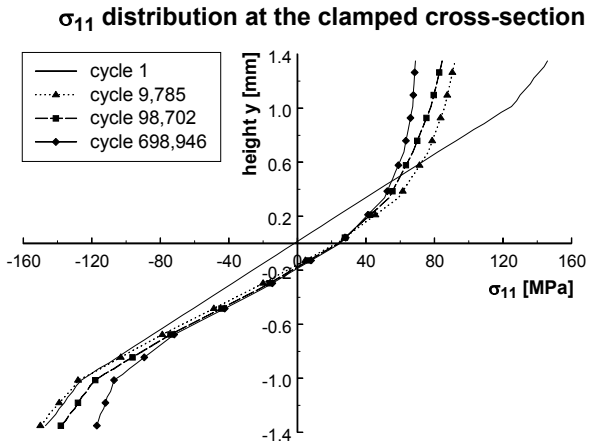

Fig. 6. Simulated distribution of σ_{11} at the clamped cross-section for the $[\#45°]_8$ specimen Pr06_3 (u_{max} = 38.9 mm).

It is obvious that the distribution of the stress σ_{22} is the same, since the principal material axes $\vec{e}_{11}$ and $\vec{e}_{22}$ of the $[\#45°]_8$ specimens are situated symmetrically with respect to the loading direction.

6. CONCLUSIONS

From experimental observations, it was concluded that fatigue damage can give rise to several phenomena in fibre-reinforced plastics: (gradual) stiffness degradation, varying displacement profile in bending, accumulation of permanent strain.

If one is interested in the growth of these phenomena, and not only in the moment of failure (i.e. the number of cycles to failure), then a damage model must be established. The fatigue damage model in this paper was based on a continuum damage mechanics approach, where selected damage variables are representing the stiffness degradation and their effect on the elastic properties. Combined with a modified interpretation of the Tsai-Wu failure criterion, the model is able to simulate the fatigue behaviour from the first loading cycle up to final failure.

ACKNOWLEDGEMENTS

The author W. Van Paepegem gratefully acknowledges his finance through a grant of the Fund for Scientific Research – Flanders (F.W.O.), and the advice and technical support of the SAMTECH company. The authors also express their gratitude to Syncoglas for their support and technical collaboration.

References

1. **Degrieck, J.** and **Van Paepegem, W.**, "Fatigue Damage Modelling of Fibre-Reinforced Composite Materials: Review", *Applied Mechanics Reviews*, 54(4), 279-300, 2001.
2. **Lawrence Wu, C.M.**, "Thermal and mechanical fatigue analysis of CFRP laminates", *Composite Structures*, 25, 339-344, 1993.
3. **Jen, M.-H.R.** and **Lee, C.-H.**, "Strength and life in thermoplastic composite laminates under static and fatigue loads. Part I: Experimental", *International Journal of Fatigue*, 20(9), 605-615, 1998.
4. **Jen, M.-H.R.** and **Lee, C.-H.**, "Strength and life in thermoplastic composite laminates under static and fatigue loads. Part II: Formulation", *International Journal of Fatigue*, 20(9), 617-629, 1998.
5. **Philippidis, T.P.** and **Vassilopoulos, A.P.**, "Fatigue strength prediction under multiaxial stress", *Journal of Composite Materials*, 33(17), 1578-1599, 1999.
6. **Talreja, R.**, "Stiffness properties of composite laminates with matrix cracking and interior delamination", *Engineering Fracture Mechanics*, 25(5/6), 751-762, 1986.

7. **Talreja, R.**, "Damage mechanics of composite materials based on thermodynamics with internal variables", Durability of polymer based composite systems for structural applications. Proceedings of the International Colloquium, 27-31 August 1990, Brussels, Belgium, Elsevier, pp. 65-79, 1990.
8. **Allen, D.H.**, **Harris, C.E.** and **Groves, S.E.**, "A thermomechanical constitutive theory for elastic composites with distributed damage - I. Theoretical development", *International Journal of Solids and Structures*, 23(9), 1301-1318, 1987.
9. **Allen, D.H.**, **Harris, C.E.** and **Groves, S.E.**, "A thermomechanical constitutive theory for elastic composites with distributed damage - II. Application to matrix cracking in laminated composites", *International Journal of Solids & Structures*, 23(9), 1319-1338, 1987
10. **Sedrakian, A.**, **Ben Zineb, T.**, **Billoet, J.L.**, **Sicot, N.** and **Lardeur, P.**, "A numerical model of fatigue behaviour for composite plates: application to a three point bending test", International Conference on fatigue of composites. Proceedings, 3-5 June 1997, Paris, France, La Société Française de Métallurgie et de Matériaux, pp. 415-423, 1997.
11. **Sedrakian, A.**, **Ben Zineb, T.**, **Billoet, J.L.**, **Sicot, N.** and **Lardeur, P.**, "Fatigue behaviour simulation of industrial composite parts", Proceedings of the Second International Conference on Fatigue of Composites. 4-7 June 2000, Williamsburg, pp. 4.5-4.6, 2000.
12. **Shokrieh, M.M.** and **Lessard, L.B.**, "Multiaxial fatigue behaviour of unidirectional plies based on uniaxial fatigue experiments - I. Modelling", *International Journal of Fatigue*, 19(3), 201-207, 1997.
13. **Shokrieh, M.M.** and **Lessard, L.B.**, "Multiaxial fatigue behaviour of unidirectional plies based on uniaxial fatigue experiments - II. Experimental evaluation", *International Journal of Fatigue*, 19(3), 209-217, 1997.
14. **Lubin, G.** and **Dastin, S.J.**, "Aerospace applications of composites", Handbook of Composites. New York, Van Nostrand Reinhold Company Inc., pp. 722-743, 1992.
15. **Bailie, J.A.**, "Woven fabric aerospace structures", Handbook of Composites. Volume 2 : Structures and design. Amsterdam, Elsevier, pp. 353-391, 1989.
16. **Degrieck, J.**, **Van Paepegem, W.** and **Boone, P.**, "Application of digital phase-shift shadow Moiré to micro deformation measurements of curved surfaces", *Optics and Lasers in Engineering*, 36, 29-40, 2001.
17. **Van Paepegem, W.**, "Development and finite element implementation of a damage model for fatigue of fibre-reinforced polymers", Ph.D. thesis. Gent, Belgium, Ghent University Architectural and Engineering Press (ISBN 90-76714-13-4), 403 p., 2002.
18. **Van Paepegem, W.** and **Degrieck, J.**, "Calculation of Damage-dependent Directional Failure Indices from the Tsai-Wu Static Failure Criterion", *Composites Science and Technology*, 63(2), 305-310, 2002.